Supporting Information Appendix
For
Evolution of Photoreceptors in a Diurnal Garter Snake (*Thamnophis proximus*): What Happened to the Rods in the All-Cone Retina?

Ryan K. Schott, Johannes Müller, Clement G. Y. Yang, Nihar Bhattacharyya, Natalie Chan, Mengshu Xu, James M. Morrow, Ana-Hermina Ghenu, Ellis R. Loew, Vincent Tropepe, and Belinda S. W. Chang

Table of Contents

SI Results

***Thamnophis proximus* possesses three visual pigments.** Previous MSP on *Python regius* (ball python) and *Boa constrictor imperator* (common northern boa), both of which are nocturnal, found three visual pigments in three cone types (1, 2). A long-wavelength pigment with a λ_{max} of 551 and 549 nm, respectively, was found in large single cones (1, 2), an 8–10 nm red-shift relative to *T. proximus*, but similar to the value for *T. sirtalis*. Double cones are not present in python or boa retinas. In small single cones a short-wavelength pigment was found with a λ_{max} of 360 and 357 nm, respectively for *Python* and *Boa* (1, 2), a 6–9 nm blue-shift relative to *T. proximus*, but again similar to the value for *T. sirtalis*. The third pigment was rhodopsin, found in rod cells, with a λ_{max} of 494 and 495 (1, 2).

Recently MSP was performed on two species of sea snakes (3). Sea snakes are caenophidian snakes that belong to the family Elapidae and are more closely related to colubrid snakes than they are to pythons and boas. The pattern of cell types in the sea snakes is very similar to that found for *Thamnophis* with double cones, large single cones, and two types of small single cones. Three visual pigments were identified: A long-wavelength pigment with a λ_{max} of 555–559 nm was found in the large single cones and double cones. A medium-wavelength pigment with a λ_{max} of 496 nm was found in one of the types of small single cones and a short-wavelength pigment with a λ_{max} of 428–430 nm was found in in the other type (3). The λ_{max} of the long-wavelength pigment is very similar to *Thamnophis* and to pythons and boas, but that of the short-wavelength pigment, if it is the same pigment present in these snakes, is red-shifted into the violet. This would be the first incidence of a violet-type SWS1 in non-avian reptiles, as other non-avian reptile SWS1 pigments, including *Thamnophis*, are UV-type (4). The authors suggest that this may be an adaptation resulting from the attenuation of short

wavelengths with increased depth (3). The λ_{max} of the middle-wavelength pigment is very similar to the rhodopsin pigment of pythons and boas suggesting that it is rhodopsin, but this pigment is expressed in cones (3). Measurements of the middle-wavelength single cones show that they have smaller ellipsoids than expected, which the authors suggest may be evidence that they are 'transmuted' rods. Whether the middle-wavelength pigment identified in *Thamnophis*, and in the sea snakes, is rhodopsin cannot be determined from MSP data alone.

Rhodopsin and rod transducin are expressed in cone photoreceptor cells.

In light of our results, previously unexplained staining of *T. sirtalis* retina by Sillman et al. (5) is consistent with the expression of rhodopsin in the all-cone retina. Sillman et al. (5) performed immunohistochemical staining of *T. sirtalis* retina using a variety of different antibodies including three raised against rhodopsin (AO, B6, and K42-41), but did not stain for rod transducin. Using this approach, they identified two distinct populations of small single cones, one that reacted strongly with AO, B6 and B42-41 and one that reacted only weakly or not at all (5). Based on our results, we can conclude that the population of cones that reacted strongly with AO, B6, and B42-41 (the three antibodies raised against rhodopsin) were likely rhodopsin-expressing cones homolgous to those identified here in *T. Proximus*. Combined with our MSP, sequencing, and *in vitro* expression results, the immunohistochemical results of both Sillman et al. (5) and the present study strongly support the hypothesis that *Thamnophis* rhodopsin is expressed in a 'cone' cell that is actually derived from a rod.

SI Materials and Methods

Animals. Adult *Thamnophis proximus* were obtained from a licensed retailer and euthanized using approved procedures. Eyes were extracted and prepared either for MSP, RNA extraction, or electron microscopy. Blood was collected for genomic DNA extraction.

Microspectrophometry. Methodology used for MSP measurements and analyses has been described previously (Loew, 1994; Sillman et al., 1997). Briefly, after dark adaptation, snakes were sacrificed and the retinas were extracted and fixed on slides. Absorbance spectra of individual photoreceptor cells were measured, and plotted into absorption curves, from which the sensitivity range and wavelength of maximum absorption was inferred (Loew, 1994; Sillman et al., 1997).

Opsin isolation and sequencing. Total mRNA was extracted from *Thamnophis proximus* eye tissue using the Qiagen RNeasy kit and QiaShredder columns. cDNA libraries were constructed using the SMART cDNA Library Construction Kit (Clontech). Genomic DNA was extracted using QIAamp Blood Minikit. Degenerate primers were designed from an alignment of tetrapod RH1 and RH2, LWS, and SWS1 genes (Table 1). Hot start Taq DNA polymerases AmpliTaq Gold (Applied Biosystems) or FastStart (Roche) were used under standard PCR conditions. Reactions were visualized on agarose gels and DNA fragments extracted and purified (Qiagen QIAquick). Gene fragments were cloned and ligated into TOPO-TA vectors (Invitrogen) or pJET (Fermentas) and transformed into One Shot TOP10 or Mach1 competent cells (Invitrogen). Sequencing was performed with BigDye Terminator (ABI) reagents in the forward and reverse

directions on a 3730 DNA Analyzer (Applied Biosystems). To minimize artifacts from sequencing, multiple clones were sequenced and sequencing errors and ambiguities were eliminated. To obtain 5’ and 3’ ends, RACE (rapid amplification of cDNA ends) was performed with specific, nested primers designed based on the sequenced fragments of each gene (Table S1). RACE was performed using the SMART RACE cDNA amplification kit (Clontech) under standard conditions. GenomeWalker (Clontech) was additionally used to initially obtain the 5' end of RH1.

Phylogenetic and molecular evolutionary analyses. A representative set of vertebrate rhodopsin (RH1), LWS, and SWS1 sequences was obtained from Genbank. These sequences were aligned with the RH1, LWS, and SWS1 genes sequenced from *Thamnophis proximus* using PAGAN codon alignment (6). The poorly aligned 5' and 3' ends of the sequence were manually trimmed. In order to confirm the identities of the genes from *T. proximus*, gene trees were estimated using the resulting PAGAN alignments in MrBayes 3 (7, 8) using reversible jump MCMC with a gamma rate parameter (nst=mixed, rates=gamma), which explores the parameter space for the nucleotide model and the phylogenetic tree simultaneously. The analyses were each run for five million generations with a 25% burn-in. Convergence was confirmed by checking that the standard deviations of split frequencies approached zero and that there was no obvious trend in the log likelihood plot. The RH1 gene tree was used to further analyze the evolution of *T. proximus*, and other snake, rhodopsins.

To estimate the strength and form of selection acting on RH1, the gene tree and alignment were analyzed with the codeml package of PAML 4 (9) using the random sites models (M0, M1a, M2a, M3, M7, M8a, and M8), branch and branch-site model (10), and clade model C (CmC) (11). Comparisons between the PAML random sites models were used to test for

variation in ω (M3 vs M0) and for the presence of a positively selected class of sites (M2a vs M1a, and M8 vs M7 and M8a). All analyses were repeated at least three times with varying initial starting points of κ (transition to transversion rate ratio) and ω (the synonymous to nonsynomymous rate ratio, d_N/d_S) to avoid potential local optima. The model pairs were compared using a likelihood ratio test (LRT) with a χ^2 distribution.

The branch, branch-site, and clade models were used to test for changes in selective constraint and positive selection in snakes, caenophians, and *T. proximus* by placing them in a separate foreground partition. The branch model estimates a single ω value for each branch and/or clade type specified a priori. This model is useful for testing for overall changes in selective constraint between branches/clades. The branch-site and clade models allow ω to vary both among sites and between branches/clades. The branch-site model has four site classes: 0) $0 < \omega_0 < 1$ for all branches; 1) $\omega_2 = 1$ for all branches, 2a) $\omega_{2a} = \omega_{2b} \geq 1$ in the foreground and $0 < \omega_{2a} = \omega_0 < 1$ in the background, and 2b) $\omega_{2b} = \omega_{2a} \geq 1$ in the foreground and $\omega_{2b} = \omega_2 = 1$ in the background. This model provides a test for positive selection on specified branches/clades. CmC assumes that some sites evolve conservatively across the phylogeny (two classes of sites where $0 < \omega_0 < 1$ and $\omega_1 = 1$), while a class of sites is free to evolve differently among two or more partitions (e.g., $\omega_{D1} > 0$ and $\omega_{D1} \neq \omega_{D2} > 0$), which can be branches, clades, or a mix of both. Rather than a test for positive selection, this provides a test for divergent selective pressure (although a test for positive selection can be performed if desired; see (12)). For further explanation of the methods and partitioning see Schott et al. (13).

Rhodopsin expression and spectroscopic assay. The full length RH1 sequence was amplified from cDNA and inserted in the pJET1 cloning vector (Fermentas). The sequence was re-amplified using primers that added the BamHI and EcoRI restriction sites to its 5' and 3' ends,

respectively, and inserted into the p1D4-hrGFP II expression vector following Morrow and Chang (2010). Expression vectors containing *T. proximus* rhodopsin were transiently transfected into cultured HEK293T cells using Lipofectamine 2000 (Invitrogen; 12 µg of DNA per 10-cm plate) and harvested after 48 h. A total of 48 plates were used and concentrated using a Centrifugal Filter Device (Amicon). Visual pigments were regenerated with 11-cis-retinal, solubilized in 1% n-dodecyl-β-D-maltoside, and purified with the 1D4 monoclonal antibody as previously described (14, 15). The ultraviolet-visible absorption spectra of purified visual pigments were recorded using a Cary 4000 double beam spectrophotometer (Aglient). Dark-light difference spectra were calculated by subtracting light-bleached absorbance spectra from respective dark spectra. Pigments were photoexcited with light from a fiber optic lamp (Dolan-Jenner) for 60s at 25°C.

Immunohistochemistry. Four retinas from two dark-adapted *T. proximus* were processed for immunohistochemistry. Retinas from CD-1 mice were processed as a positive control. After enucleation of eyes in the light, the eyecups were fixed overnight at 4ºC in 4% paraformaldehyde in PBS. Eyes were then infiltrated with increasing concentrations of sucrose in PBS and embedded in a 2:1 solution of 30% sucrose and O.C.T compound (Tissue-Tek) at -20ºC. The eyes were cryosectioned transversely into 20 µm sections using a Leica CM3050 cryostat. Sections were blocked in 2% normal goat serum with 1% BSA in PDT for 1 h, incubated with primary antibody diluted in blocking solution overnight at 4ºC, and then secondary antibody for 1 h at 37ºC. Sections were stained with 10 µg/mL Hoechst (Jackson Immunoresearch) and mounted with ProLong Gold Antifade mounting media (Life Technologies). Sections were visualized via a Leica TCSSP8 confocal laser microscope. Primary antibodies used were the K20 antibody (Santa Cruz Biotechnology) and 4D2 anti-rhodopsin antibody. AlexaFluor-488 goat

anti-rabbit (Life Technologies Inc.) and the Cy-3 anti-mouse (Jackson Immunoresearch) were used as secondary antibodies.

The antibody used to detect rhodopsin, 4D2, is a monoclonal mouse antibody raised against the N-terminal domain of bovine rhodopsin. It has been shown to selectively label rod outer segments, but not cone outer segments (16). This specificity has been shown for a wide variety of vertebrates including mammals (16, 17), fish (18), amphibians (16, 19, 20), and reptiles (21-23). Furthermore its specificity has been verified in squamates through immunoblotting of anole retina (22).

The rod transducin antibody we used, K20, is an affinity purified rabbit polyclonal antibody raised against amino acid positions 75-125 of the $G\alpha t_1$ subunit of the human rod G protein transducin. K20 has been shown to be specific for rods in both mammalian (24-26) and non-mammalian (27) species without any labelling of cone cells, and has been used to calculate expression of rod transducin in zebrafish retina through immunoblotting (28) and for labelling of rod transducin in *Xenopus* rods (29).

Electron microscopy. Eight *T. proximus* retinae were prepared for SEM and two for TEM. Eyes were hemisected and the retina separated from its pigmented epithelium. Retinas were fixed in 3% glutaraldehyde overnight at room temperature, rinsed with phosphate buffer (0.1 M, pH 7.8) and postfixed in 1.0% osmium tetroxide for 1 h at room temperature. The retina was then dehydrated with increasing concentrations of ethanol. Tissues for SEM were infiltrated with a Hexamethyldisilizane (HMDS) series and allowed to volatilize overnight. The retina was then positioned with the photoreceptors facing outward and Sputter coated with gold-palladium using the Bal24 Tec SCD050. The sample was examined with the Hitachi S2500 at 20 kV and images acquired using a Quartz PCI. Tissues for TEM were embedded with modified Spurr's epoxy

resin. Semithin sections (0.51 µm) were stained with Toluidine blue (Fisher BioReagents) and methylene blue (British Drug House) and ultrathin sections (60–90 nm) were stained with 3% uranyl acetate in 50% methanol and post-stained with Reynold's lead citrate. Sections were examined with the Hitachi H7000 at 75 kV and images acquired using an AMT 11 megapixel digital camera.

SI References

1. Sillman AJ, Carver JK, & Loew ER (1999) The photoreceptors and visual pigments in the retina of a boid snake, the ball python (*Python regius*). *J Exp Biol* 202(14):1931-1938.
2. Sillman AJ, Johnson JL, & Loew ER (2001) Retinal photoreceptors and visual pigments in *Boa constrictor imperator*. *J Exp Zool* 290(4):359-365.
3. Hart NS, Coimbra JP, Collin SP, & Westhoff G (2012) Photoreceptor types, visual pigments, and topographic specializations in the retinas of hydrophiid sea snakes. *J Comp Neurol* 520(6):1246-1261.
4. Hauser FE, van Hazel I, & Chang BS (2014) Spectral tuning in vertebrate short wavelength-sensitive 1 (SWS1) visual pigments: can wavelength sensitivity be inferred from sequence data? *J Exp Zool B Mol Dev Evol* 322(7):529-539.
5. Sillman AJ, Govardovskii VI, Rohlich P, Southard JA, & Loew ER (1997) The photoreceptors and visual pigments of the garter snake (*Thamnophis sirtalis*): a microspectrophotometric, scanning electron microscopic and immunocytochemical study. *J Comp Phys A* 181(2):89-101.
6. Löytynoja A, Vilella AJ, & Goldman N (2012) Accurate extension of multiple sequence alignments using a phylogeny-aware graph algorithm. *Bioinformatics* 28(13):1684-1691.
7. Ronquist F & Huelsenbeck JP (2003) MrBayes 3: Bayesian phylogenetic inference under mixed models. *Bioinformatics* 19(12):1572-1574.
8. Ronquist F, *et al.* (2012) MrBayes 3.2: efficient Bayesian phylogenetic inference and model choice across a large model space. *Syst Biol* 61(3):539-542.

9. Yang Z (2007) PAML 4: phylogenetic analysis by maximum likelihood. *Mol Biol Evol* 24(8):1586-1591.

10. Zhang J, Nielsen R, & Yang Z (2005) Evaluation of an improved branch-site likelihood method for detecting positive selection at the molecular level. *Mol Biol Evol* 22(12):2472-2479.

11. Bielawski JP & Yang Z (2004) A maximum likelihood method for detecting functional divergence at individual codon sites, with application to gene family evolution. *J Mol Evol* 59(1):121-132.

12. Chang BSW, *et al.* (2012) The future of codon models in studies of molecular function: ancestral reconstruction and clade models of functional divergence. *Codon evolution: mechanisms and models*, eds Cannarozii GM & Schneider A (Oxford University Press, Oxford), pp 145-163.

13. Schott RK, Refvik SP, Hauser FE, Lopez-Fernandez H, & Chang BS (2014) Divergent positive selection in rhodopsin from lake and riverine cichlid fishes. *Mol Biol Evol* 31(5):1149-1165.

14. Morrow JM & Chang BS (2010) The p1D4-hrGFP II expression vector: a tool for expressing and purifying visual pigments and other G protein-coupled receptors. *Plasmid* 64(3):162-169.

15. Morrow JM, Lazic S, & Chang BS (2011) A novel rhodopsin-like gene expressed in zebrafish retina. *Vis Neurosci* 28(4):325-335.

16. Hicks D & Molday RS (1986) Differential immunogold dextran labeling of bovine and frog rod and cone cells using monoclonal-antibodies against bovine rhodopsin. *Exp Eye Res* 42(1):55-71.

17. Hicks D, Sparrow J, & Barnstable CJ (1989) Immunoelectron microscopical examination of the surface distribution of opsin in rat rod photoreceptor cells. *Exp Eye Res* 49(1):13-29.

18. Knight JK & Raymond PA (1990) Time course of opsin expression in developing rod photoreceptors. *Development* 110(4):1115-1120.

19. Bugra K, Jacquemin E, Ortiz JR, Jeanny JC, & Hicks D (1992) Analysis of opsin messenger-rna and protein expression in adult and regenerating newt retina by immunology and hybridization. *J Neurocytol* 21(3):171-183.

20. Ma JX, *et al.* (2001) A visual pigment expressed in both rod and cone photoreceptors. *Neuron* 32(3):451-461.

21. Bennis M, *et al.* (2005) Rhodopsin-like immunoreactivity in the 'all cone' retina of the chameleon (Chameleo chameleo). *Exp Eye Res* 80(5):623-627.

22. McDevitt DS, Brahma SK, Jeanny JC, & Hicks D (1993) Presence and foveal enrichment of rod opsin in the all-cone retina of the american chameleon. *Anat Rec* 237(3):299-307.

23. New ST, Hemmi JM, Kerr GD, & Bull CM (2012) Ocular anatomy and retinal photoreceptors in a skink, the sleepy lizard (Tiliqua rugosa). *Anat Rec (Hoboken)* 295(10):1727-1735.

24. Elias R, Sezate S, Cao W, & McGinnis J (2004) Temporal kinetics of the light/dark translocation and compartmentation of arrestin and alpha-transducin in mouse photoreceptor cells. *Mol Vis* 10(81):672-681.

25. Lobanova ES, *et al.* (2010) Mechanistic basis for the failure of cone transducin to translocate: why cones are never blinded by light. *J Neurosci* 30(20):6815-6824.

26. Saïdi T, Mbarek S, Chaouacha-Chekir RB, & Hicks D (2011) Diurnal rodents as animal models of human central vision: characterisation of the retina of the sand rat Psammomys obsesus. *Graefes Arch Clin Exp Ophthalmol* 249(7):1029-1037.

27. Wada Y, Okano T, & Fukada Y (2000) Phototransduction molecules in the pigeon deep brain. *J Comp Neurol* 428(1):138-144.

28. Vogalis F, *et al.* (2011) Ectopic expression of cone-specific G-protein-coupled receptor kinase GRK7 in zebrafish rods leads to lower photosensitivity and altered responses. *J Physiol* 589(Pt 9):2321-2348.

29. Kerov V & Artemyev NO (2011) Diffusion and light-dependent compartmentalization of transducin. *Mol Cell Neurosci* 46(1):340-346.

30. Castoe TA, *et al.* (2013) The Burmese python genome reveals the molecular basis for extreme adaptation in snakes. *Proc Natl Acad Sci U S A* 110(51):20645-20650.

SI Figures

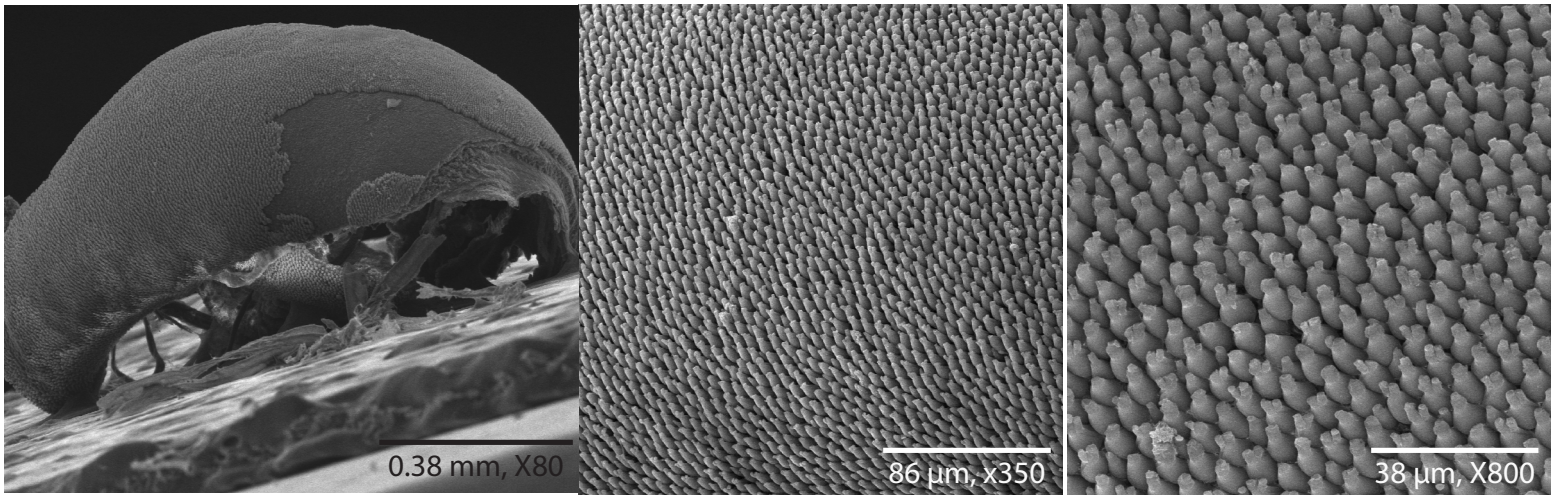

Figure S1. Scanning electron microscope images of *Thamnophis proximus* retina at increasing magnifications illustrating the all-cone photoreceptor population.

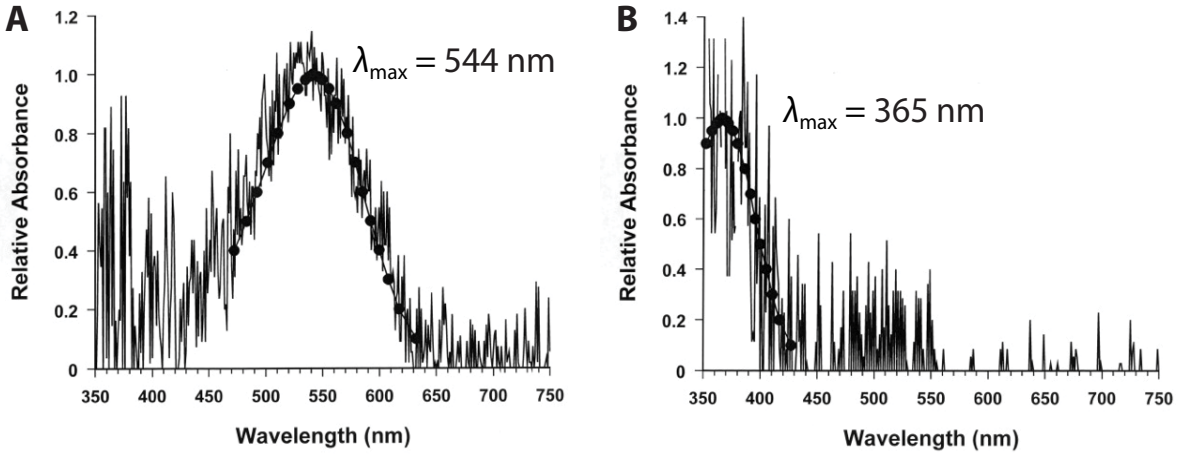

Figure S2. Normalized visual pigment absorbance spectra measured using microspectrophometry (MSP) on intact photoreceptor cells from the long- (**A**) and short- (**B**) wavelength visual pigments of *Thamnophis proximus*. The filled circles and smooth curves are for the best-fit visual pigments calculated from vitamin-A1-based template data. The λ_{max} values are the average of measurements from multiple cells as shown in Table S1.

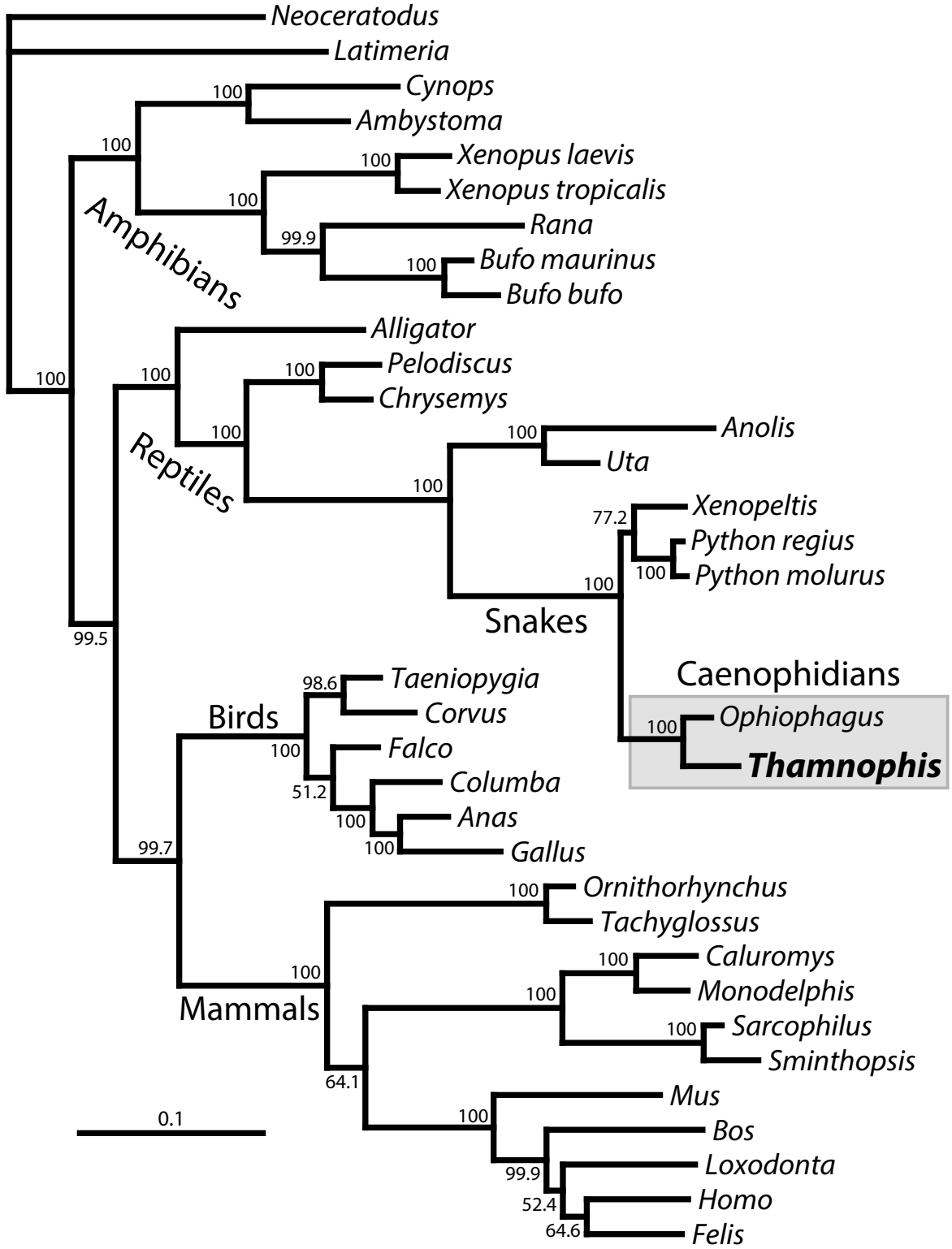

Figure S3. Rhodopsin gene tree estimated using Bayesian inference illustrating the position of *Thamnophis proximus* RH1. This tree topology was used for the selection analyses. Numbers at the nodes are posterior probability percentages.Species [Genbank accession number]: *Alligator mississippiensis* [U23802], *Ambystoma tigrinum* [U36574], *Anas platyrhynchos* [XM_005012054], *Anolis carolinensis* [L31503], *Bos taurus* [NM_001014890], *Bufo bufo* [U59921], *Bufo maurinus* [U59922], *Caluromys philander* [AY313946], *Chrysemys picta belli* [XM_008168043], *Columba livia* [AF149230], *Corvus macrorhynchos* [AB555651], *Cynops pyrrhogaster* [AB043890], *Falco cherrug* [XM_005443603], *Felis catus* [NM_001009242], *Gallus gallus* [NM_001030606], *Homo sapiens* [NM_000539], *Latimeria chalumnae* [AF131253], *Loxodonta africana* [NM_001280858], *Monodelphis domestica* [XM_001366188], *Mus musculus* [NM_145383], *Neocratodus forsteri* [EF526295], *Ophiophagus hannah* (30), *Ornithorhynchus anatinus* [NM_001127627], *Pelodiscus sinensis* [XM_006132837], *Python molurus bivittatus* (30), *Python regius* [FJ497236], *Rana temporaria* [U59920], *Sarcophilus harrisii* [XM_003762449], *Sminthopsis crassicaudata* [AY159786], *Tachyglossus aculeatus* [JX103830], *Taeniopygia guttata* [NM_001076695], *Thamnophis proximus* [This study: XXXXXX], *Uta stansburiana* [DQ100325], *Xenopeltis unicolor* [FJ497233], *Xenopus laevis* [NM_001087048], *Xenopus tropicalis* [NM_001097334].

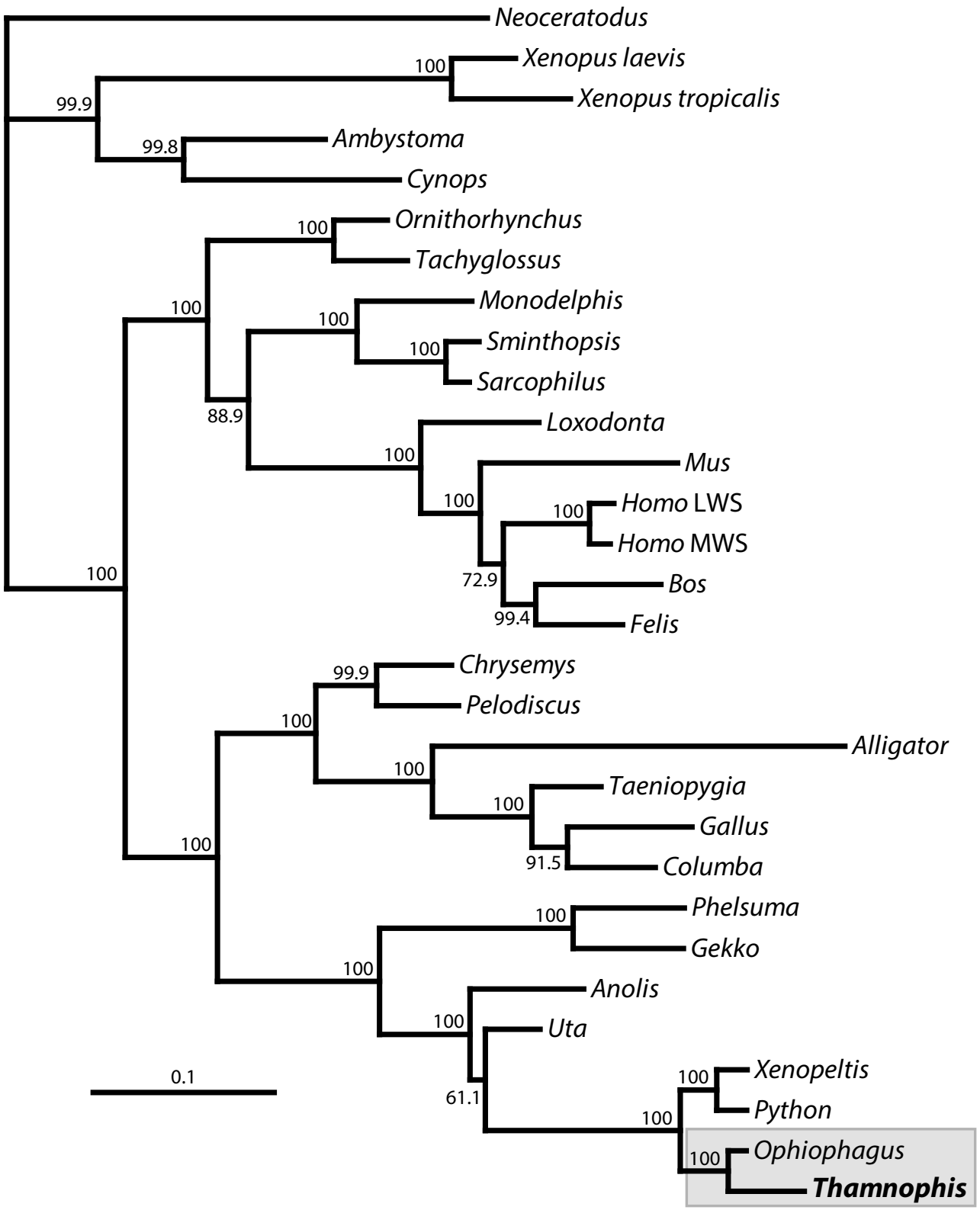

Figure S4. LWS gene tree estimated using Bayesian inference illustrating the position of *Thamnophis proximus*. Numbers at the nodes are posterior probability percentages. Species [Genbank accession number]: *Alligator mississippiensis* [XM_006269029], *Ambystoma tigrinum* [AF038947], *Anolis carolinensis* [XM_008103916], *Bos taurus* [NM_174566], *Chrysemys picta belli* [XM_005281282], *Columba livia* [AH007800], *Cynops pyrrhogaster* [AB043891], *Felis catus* [NM_001009871], *Gallus gallus* [NM_205440], *Gekko gecko* [M92036], *Homo sapiens* LWS [NM_020061], *Homo sapiens* MWS [NM_000513], *Loxodonta africana* [NM_001280862], *Monodelphis domestica* [NM_001145081], *Mus musculus* [NM_008106], *Neocratodus forsteri* [EF526297], *Ophiophagus hannah* (30), *Ornithorhynchus anatinus* [NM_001127625], *Pelodiscus sinensis* [XM_006113208], *Phelsuma madagascariensis longintinue* [AF074043], *Python regius* [FJ497238], *Sarcophilus harrisii* [XM_003774721], *Sminthopsis crassicaudata* [EU232013], *Tachyglossus aculeatus* [EU636011], *Taeniopygia guttata* [AF222333], *Thamnophis proximus* [This study: XXXXXX], *Uta stansburiana* [DQ129869], *Xenopeltis unicolor* [FJ497235], *Xenopus laevis* [NM_001090645], *Xenopus tropicalis* [NM_001102861].

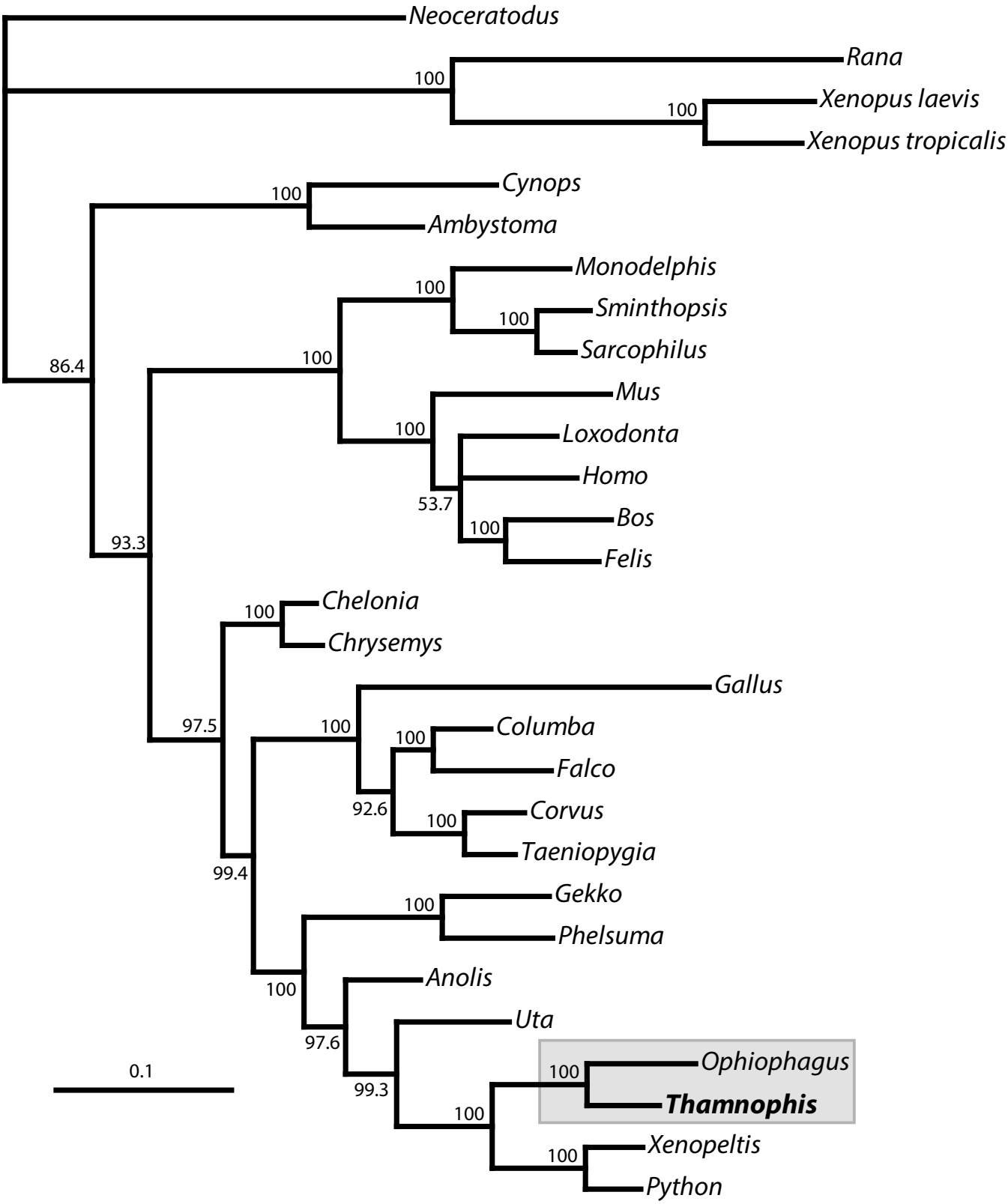

Figure S5. SWS1 gene tree estimated using Bayesian inference illustrating the position of *Thamnophis proximus*. Numbers at the nodes are posterior probability percentages. Species [Genbank accession number]: *Alligator mississippiensis* [], *Ambystoma tigrinum* [AF038948], *Anolis carolinensis* [AH007736], *Bos taurus* [NM_174567], *Chelonia mydas* [XM_007067421], *Chrysemys picta belli* [XM_005281289], *Columba livia* [AH007798], *Corvus brachyrhynchos* [XM_008637700], *Cynops pyrrhogaster* [AB052889], *Falco cherrug* [XM_005446545], *Felis catus* [BK006813], *Gallus gallus* [NM_205438], *Gekko gecko* [AY024356], *Homo sapiens* [NM_001708], *Loxodonta africana* [NM_001280859], *Monodelphis domestica* [NM_001145084], *Mus musculus* [NM_007538], *Neocratodus forsteri* [EF526298], *Ophiophagus hannah* (30), *Phelsuma madagascariensis longintinue* [AF074045], *Python regius* [FJ497237], *Rana catesbeiana* [AB001983], *Sarcophilus harrisii* [XM_003771592], *Sminthopsis crassicaudata* [AY442173], *Taeniopygia guttata* [AF222331], *Thamnophis proximus* [This study: XXXXXX], *Uta stansburiana* [DQ100325], *Xenopeltis unicolor* [FJ497234], *Xenopus laevis*

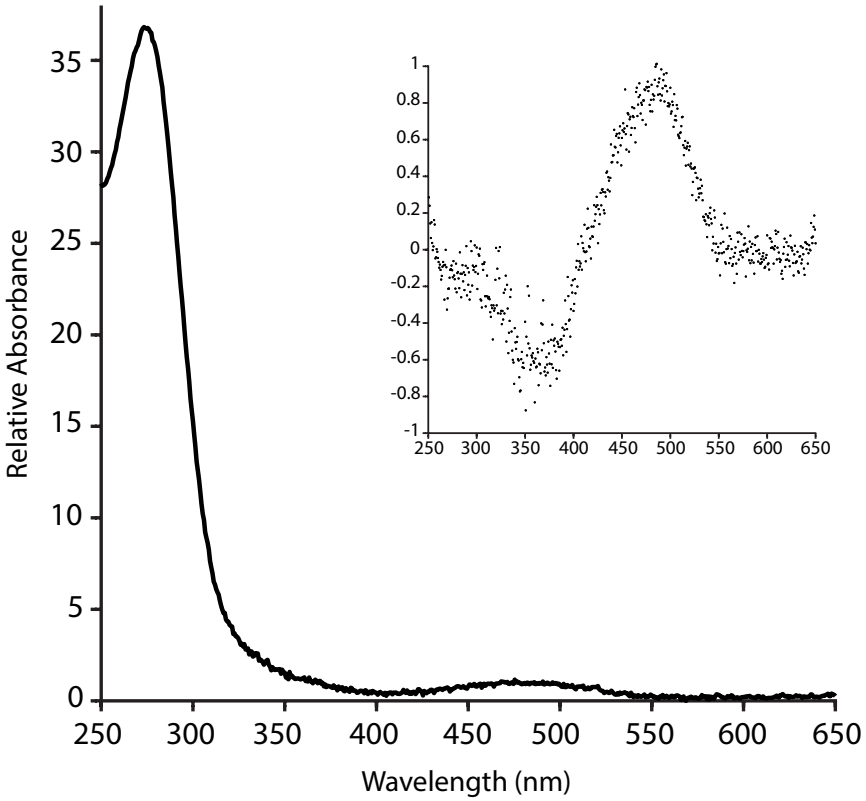

Figure S6. Dark absorption spectrum of *in vitro* expressed *Thamnophis proximus* rhodopsin. **Inset**, light-dark difference spectrum.

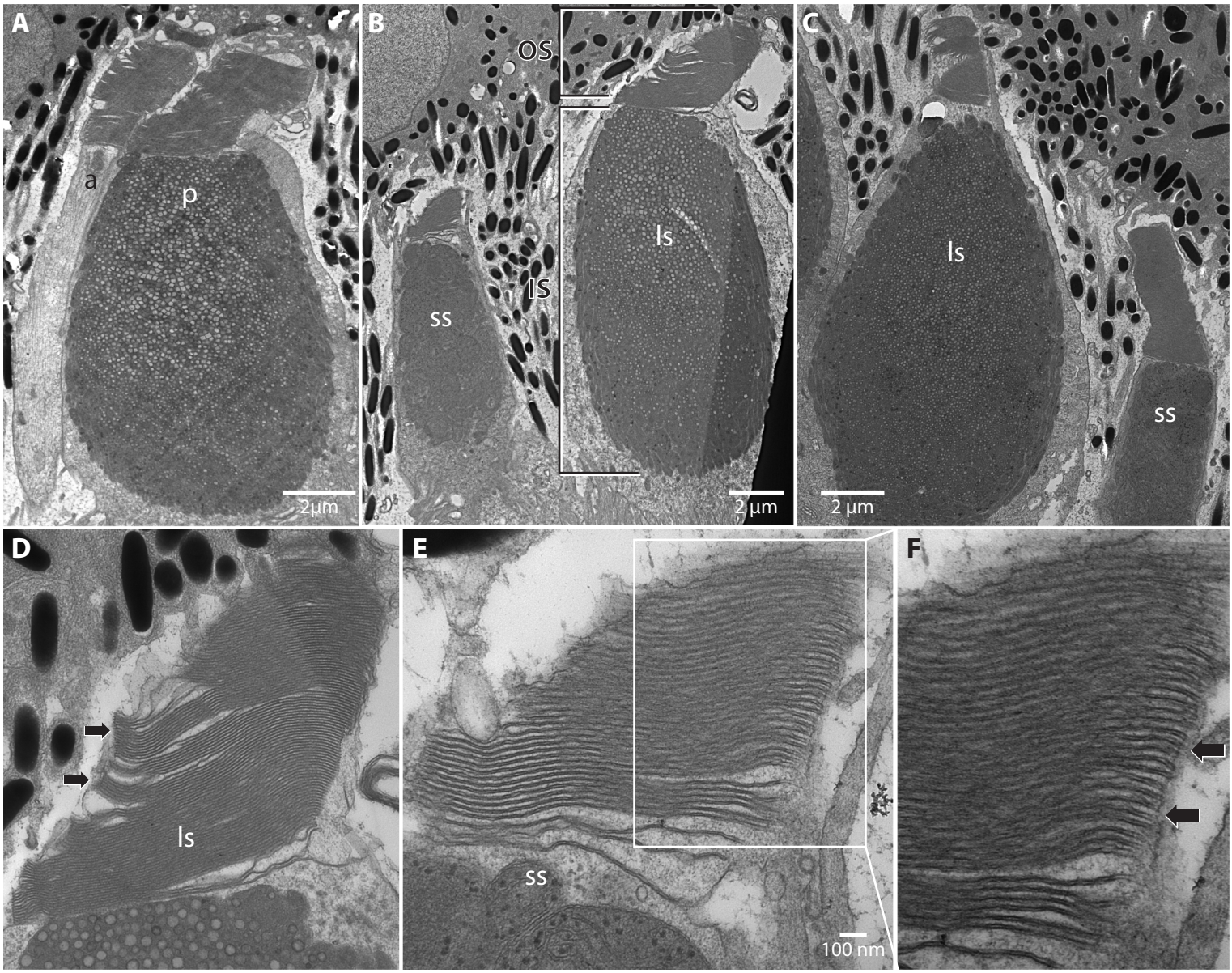

Figure S7. Transmission electron microscope (TEM) images of *Thamnophis proximus* photoreceptor cells. **A**, double cone showing accessory (**a**) and principal (**p**) members. **B**, large single cone (**ls**) and small single cone (**ss**), with the inner (**IS**) and outer (**OS**) segments of the photoreceptor cell demarcated. Note the short, tapering outer segments and large, bulbous inner segments. **C**, large single cone and small single cone of a different type. Note that this type of small single cone has a more rod-like outer segment, and much less bulbous inner segment. **D–F**, close-ups of the outer segments of a large single cone (**D**) and small single cone of the first type (**E,F**), noting the lamellar structure of the open discs (**arrows**).

SI Tables

Table S1. Estimates of peak absorbance (λ_{max}) from individual photoreceptor cells for each of the different cone types as measured by microspectrophotometry (MSP).

Cell Type	Pigment Type	λ_{max} of Individual Cell (nm)								Mean	SD
		1	2	3	4	5	6	7	8		
SS	UV	366	364	364	366	-	-	-	-	365	1.2
SS	MW	483	483	482	480	484	480	483	483	482	1.5
LS	LW	542	544	-	-	-	-	-	-	543	1.4
DC-P	LW	544	544	545	543	542	545	544	544	544	1.0
DC-A	LW	541	544	543	545	544	-	-	-	544	1.5

Abbreviations—**SS**, small single cone; **LS**, large single cone, **DC-P**, double cone, principal member; **DC-A**, double cone accessory member; **SD**, standard deviation.

Table S2. Results of analyses of selection of rhodopsin using PAML random sites, branch, and clade models.

Model & Foreground[1]	*ln*L	Parameters[2]			Null	*p* [df][3]
		ω_0/p	ω_1/q	$\omega_2/\omega_p/\omega_d$		
M0	-12378.0	0.07287	-	-	N/A	-
M1a	-12227.8	0.056 (94.1%)	1 (5.9%)	-	M0	0.000* [1]
M2a	-12227.8	0.06 (94.1%)	1 (4.6%)	1 (1.3%)	M1a	1 [2]
M2a_rel	-12030.6	0.00 (63%)	1 (2%)	0.17 (35%)	M1a	0.000* [2]
M3	-12022.9	0.00 (61%)	0.14 (34%)	0.55 (0.05%)	M0	0.000* [4]
M7	-12029.8	0.23	2.21	-	N/A	-
M8	-12024.2	0.25	3.20	1 (1%)	M7	0.004* [2]
Br_Snake	-12369.7	0.07 Snake: 0.05	-	-	M0	0.000* [1]
Br_Caen	-12371.2	0.07 Caen: 0.20	-	-	M0	0.000* [1]
Br_Tham	-12376.2	0.07 Tham: 0.17	-	-	M0	0.055 [1]
CmC_Snake	-12026.4	0.00 (62.7%)	1 (2.2%)	0.16 (35.1%) Snake: 0.29	M2a_rel	0.004* [1]
CmC_Caen	-12026.9	0.00 (62.6%)	1 (2.1%)	0.16 (35.1%) Caen: 0.40	M2a_rel	0.007* [1]
CmC_Tham	-12029.3	0.00 (62.6%)	1 (2.3%)	0.16 (35.1%) Tham: 0.37	M2a_rel	0.107 [1]

[1]The foreground partition is listed after the underscore for the branch and clade models and consists of either snakes (Snakes), caenophidians (Caen), or *Thamnophis proximus* (Tham). All other sequences are present in the background partition.
[2]ω values of each site class are shown are shown for model M0-M3 (ω_0– ω_2) with the proportion of each site class in parentheses. For M7 and M8, the shape parameters, p and q, which describe the beta distribution are listed instead. In addition, the ω value for the positively selected site class (ω_p, with the proportion of sites in parentheses) is shown for M8. The branch model only has a single site class (ω_0), but this is allowed to vary between the foreground and background partitions. For CmC, ω_D is the divergent site class, which has a separate value for the foreground and background partitions.
[3]Significant *p*-values ($\alpha = 0.05$) are marked with an asterisk (*). Degrees of freedom are given in square brackets after the *p*-values.
Abbreviations—***ln*L**, ln Likelihood; ***p***, *p*-value; **N/A**, not applicable.

Table S3. Primers used for isolation of *Thamnophis proximus* opsins.

Primer Name	Gene	Sequence
VertRho23F	RH1	CCCTTCGAGTATCCCCARTAYTA
VertRho113R	RH1	CCMAGMGTRGCRAAGAAGCCYTC
VertRho221R	RH1	CANASSAGGCGYCCRTAGCAGAA
SnakeRho39F	RH1	GCCTTGGCCGCGTACATGTTTCTT
SnakeRho64F	RH1	CAACACAAGAAACTCAGAACACCC
SnakeRho103R	RH1	GCATCCTACTGTCCCAAAAATGAA
VertRG168F	LWS	TGCGCTCCTCCiATHTTYGG
VertRG238F	LWS	AAGGAGTCTGARTCiACiCARAARGC
VertRG313R	LWS	GCGGAACTGTCGATTCATRAAiACRTADAT
GarterRG_5F	LWS	AAAGAGTCTGAATCAACACAGAAG
GarterRG_6F	LWS	AAAAGCGCCACCATTTACAACCCA
GarterRG_1R	LWS	CAACCGCACGGATAGCCATCCAC
GarterRG_2R	LWS	GTGAAAGGCATAGCCTGGATTGG
TetUV232F	SWS1	GCCGTGGCCGCiCARCARCARGA
AvesUV306R	SWS1	GAACTGCTTGTTCATRAARCARTA
GarterUV_12F	SWS1	GTGCTTGGGAGGATGCCCGTAGAA
GarterUV_71F	SWS1	AATATCACATCGCCCCCATGTGG
GarterUV_1075R	SWS1	TTGGTTGCGTTCCAACGTGCAGAG
GarterUV_1091R	SWS1	GGCATAGTCATCGTCTTGGTTGC